Experimental and first-principles investigation of Cr-driven color change in cesium lead halide perovskites

S. Ozen, (iD) T. Guner, G. Topcu, et al.

View Online　　**Export Citation**　　**CrossMark**

ARTICLES YOU MAY BE INTERESTED IN

AIP Publishing

Experimental and first-principles investigation of Cr-driven color change in cesium lead halide perovskites

S. Ozen,[1] T. Guner,[2] (ID) G. Topcu,[2] M. Ozcan,[1] (ID) M. M. Demir,[2] and H. Sahin[1,3,a] (ID)

AFFILIATIONS

[1]Department of Photonics, Izmir Institute of Technology, 35430 Izmir, Turkey
[2]Department of Materials Science and Engineering, Izmir Institute of Technology, 35430 Izmir, Turkey
[3]ICTP-ECAR Eurasian Center for Advanced Research, Izmir Institute of Technology, 35430 Izmir, Turkey

[a]Electronic mail: hasansahin@iyte.edu.tr

ABSTRACT

Herein, we report room temperature Cr-doping for all-inorganic perovskites that have attracted great attention in recent years due to their extraordinary optical properties, low cost, and ease of synthesis. Incorporation of Cr^{3+} ions into the perovskite crystal lattices is achieved by following a facile route involving an antisolvent recrystallization method at room temperature. It is shown that both Cr-doping and formation of crystals in the $CsPbBr_xCl_{3-x}$ phase are provided by increasing the concentration of the $CrCl_3$ solution. It is also observed that the doping procedure leads to the emergence of three types of distinctive peaks in the PL spectrum originating from $CsPbBr_xCl_{3-x}$ domains (476–427 nm), Cr-strained host lattices (515 nm), and midgap states formed by Cr dopants (675–775 nm). It is also found that the Cr-doped perovskites emitting a dark violaceous color change their color to white with a high color rendering index (88) in 30-day time intervals. Easy-tunable optical properties of all-inorganic Cs perovskites indicate their great potential for future optoelectronic device applications.

Published under license by AIP Publishing. https://doi.org/10.1063/1.5092779

I. INTRODUCTION

Lead halide perovskites ($APbX_3$, where $X = Cl^-$, Br^-, I^-) are a promising class of materials for future optoelectronic applications and are attracting much attention lately due to their outstanding photophysical[1–3] and optical[4–9] properties such as strong light absorption, high photoluminescence quantum yield, wavelength tunability, and long carrier lifetime. To date, lead halide perovskites have been obtained in the form of $APbX_3$ [where A = methylammonium (MA^+), formamidinium (FA^+), Cs^+]. Depending on the cation, these materials can be divided into two categories: organometallic and all-inorganic, where it is organometallic if the cation is MA^+ or FA^+ or all-inorganic when it is Cs^+. Among those, all-inorganic perovskites can show higher intrinsic stability due to their higher melting point ($\geq 500\,^\circ C$) and photostability compared to organometallic perovskites.[10] Starting from its first solution-process based synthesis of $CsPbBr_3$ by Protesescu et al.,[4] these materials have been applied to various kinds of devices including solar cells, LEDs, lasers, etc.[11] Meanwhile, apart from its well-known structure

as $CsPbBr_3$, various stoichiometries such as Cs_4PbBr_6 and $CsPb_2Br_5$ have also been characterized.[11,12]

Optical and electronic properties of these materials can be controlled by manipulation of their intrinsic crystal configuration such as anion-exchange[13–15] and mixed-cation[16,17] reactions. Moreover, additional control over the optical and electronic properties can be achieved via introducing dopants into a crystal system.[18–22] Doping of lead halide perovskites with the different impurities has emerged as a promising step, providing a compositional difference and structural perfection, for the alteration of many properties such as light conversion, stability, and crystal growth.[22] In addition, dopants can induce additional states in the lead halide perovskite materials, which may lead to the appearance of additional emission signals.[22–24] To date, a wide variety of impurities including alkaline-earth, rare-earth, and transition metals have been incorporated with perovskites. Among these metal dopants, divalent cations have been widely employed as Mg^{2+}, Sn^{2+}, Sr^{2+}, Cd^{2+}, or Ca^{2+} for modification of intrinsic properties of the crystals.[25,26] On the contrary, the heterovalent doping in semiconductors may also lead to switching

the sign of the majority charge carrier from n- to p-type or reverse. Therefore, one can expect heterovalent dopants as efficient elements to control the optical and electronic properties and enhance device performances of the lead halide perovskites.[27]

In this paper, motivated by the studies reporting Cr-doping driven modifications in various materials such as increasing grain,[28] metal-insulator transition,[29] acting as electron traps and retard photoinduced charge recombination, leading to enhanced photoelectrochemical activity,[30] decrease in bandgap and excitation independent luminescence,[31] the effect of Cr dopants on the structural, optical, and electronic properties of all-inorganic halide perovskites was investigated both theoretically and experimentally. First, doping Cr^{3+} ions was achieved at room temperature via the antisolvent recrystallization method. The crystallographic information of the formed perovskite crystals including both undoped and doped ones was compared, and structural changes in the presence of $CrCl_3$ were monitored. Second, the effect of incorporated Cr^{3+} ions into the host lattice on the optical and electronic characteristics of the resulting crystals was tracked through PL measurements. As a consequence of the doping process, the blue shift and additional emission peaks are observed in the presence of Cl^- and Cr^{3+} ions, respectively. It is seen that the resulting color of the material strongly depends on the Cr concentration. Afterward, the electronic band dispersion of Cr-doped perovskite crystal is calculated by density functional theory (DFT) based simulations. The resulting midgap states confirmed that the PL peaks in the red region originated from Cr atoms in the host lattice. In addition, as scanning electron microscopy (SEM) images and X-ray diffractograms put forth the phase transition, the interaction simulations of $CsPbCl_3$ and $CsPbBr_3$ structures with water elucidated the difference of degradation time.

The paper is organized as follows: experimental and theoretical methodology are given in Sec. II, results on the atomic structure are discussed in Sec. III, Cr-induced modifications in electronic and optical properties are explained in Sec. IV, environmental stability of the doped perovskite is investigated in Sec. V, and the obtained results are concluded in Sec. VI.

II. METHODOLOGY

A. Experimental methodology

1. Materials

Cesium bromide (CsBr, 99.9%, Sigma-Aldrich) and lead(II) bromide ($PbBr_2$, ≥98%, Sigma-Aldrich) were used as raw materials for all-inorganic perovskites, whereas chromium(III) chloride ($CrCl_3$, 99%, Sigma-Aldrich) was the dopant salt. Typical surfactants, namely, oleic acid (OA, 90%, Alfa Aesar) and oleylamine (OAm, 90%, Sigma-Aldrich), were employed in the solution process to obtain relatively small and stable crystals. The synthesis procedure was carried out via antisolvent recrystallization using dimethylformamide (DMF, ≥99.9%, Tekkim) and toluene (≥99%, Merck) as solvent and antisolvent, respectively. Hexane (≥98%, Sigma-Aldrich) was supplied to disperse the synthesized crystals. All reagents were purchased and used as received without any further purification.

2. Synthesis of undoped cesium lead halide perovskite

To obtain undoped lead halide perovskite, the method reported by Li *et al.* is followed.[32] After dissolving 0.4 mmol CsBr and 0.4 mmol $PbBr_2$ in 10 ml of DMF, ligands OA (1.0 ml) and OAm (0.5 ml) were added under vigorous stirring in order to obtain an ion source. 0.5 ml of the ion source that is composed of Cs^+ and Pb^{2+} was injected into 5 ml of toluene under vigorous stirring. After 3 min, the prepared mixture was centrifuged for 5 min under 6000 rpm and precipitate was redispersed in hexane.

3. Synthesis of Cr-doped cesium lead halide perovskite

To obtain Cr-doped lead halide perovskite, the method proposed by Zhu *et al.* is followed with slight modifications.[33] $CrCl_3$ (0.8 mmol) was dissolved in 10 ml of DMF to obtain dopant solution. An aliquot of precursor solution (0.5 ml) and different amounts of the chromium source (0.25 ml, 0.50 ml, and 0.75 ml and are labeled as Cr25, Cr50, and Cr75 in the text, respectively) were injected into 5 ml of toluene simultaneously under vigorous stirring to obtain chromium doped cesium lead halide perovskite NCs. The color of the solution turned to green. The color became darker as the amount of dopant solution increases. Solutions were centrifuged under 6000 rpm for 5 min. Precipitates were redispersed in hexane.

4. Characterization

The diffraction profiles of the perovskite nanocrystals were recorded with an X-ray diffractometer (XRD, X Pert Pro, Philips, Eindhoven, the Netherlands). Emission spectra were monitored by USB2000+ Spectrometer (Ocean Optics Inc., Dunedin, FL, USA) via a premium fiber cable.

B. Computational methodology

To investigate $CrCl_3$ dopant induced modifications in the structural and electronic properties of all-inorganic Cs-perovskites, density functional theory-based calculations were done by using Vienna *Ab initio* Simulation Package (VASP).[34,35] DFT calculations were performed by using the projector augmented wave (PAW)[36,37] potentials as implemented in VASP. Local density approximation (LDA)[38] including spin orbit coupling is used to describe the exchange and correlation potential.[39] The charge transfer between atoms was analyzed by the Bader technique.[40]

For plane-wave basis set, kinetic energy cutoff was taken as 500 eV for all the calculations. The total energy difference between the sequential steps as a convergence criterion for ionic relaxations was set as 10^{-5} eV. For electronic and geometric relaxations, a, b, c and positions of atoms are optimized. All structures are fully relaxed until pressure in x, y, z directions is less than $|1|$ kB. In the unit cell, the total force was reduced to a value less than 10^{-4} eV/Å. Γ-centered k-point meshes of $3 \times 3 \times 3$ were used for 20-atom cell of perovskites. Spin-polarized calculations were performed in all cases, and Gaussian smearing of 0.1 eV was used for the electronic density of states calculations.

III. CrCl₃-DRIVEN MODIFICATIONS IN ATOMIC STRUCTURE

Since all the electronic, magnetic, vibrational, and optical characteristics of materials emerge as a result of the crystal symmetry, a detailed understanding of their structural properties is of importance.

As shown in Fig. 1(a), under daylight, undoped sample has orangelike color and its appearance turns into a yellowish color upon introducing the $CrCl_3$ solution. Further increase in the additional $CrCl_3$ concentration leads to bright white color. Moreover, under the UV illumination ($\lambda = 254$ nm), undoped sample shows an intensive green emission. However, in the case of introducing the $CrCl_3$ solution, resulting emission shifts significantly toward a weak violaceous color. It is observed that such an emission remains almost unchanged with the increasing amount of $CrCl_3$ concentration.

X-ray diffraction was used to characterize the structural properties of doped and undoped samples. For the undoped crystal presented at the top of Fig. 1(d) (orange solid line), the sharp signals are observed matching with the ones of Cs_4PbBr_6.[41] On the other

hand, the addition of 0.25 ml $CrCl_3$ solution during the synthesis leads to the appearance of extra reflections in the XRD pattern of Cr25 (green solid line). These reflections substantially match with the characteristic signals of $CsPbBr_xCl_{(3-x)}$ perovskites, which are labeled with the dashed lines.[4] As shown by Guner et al., rhombus-shaped Cs_4PbBr_6 phase is an indirect semiconductor with a wide bandgap, while cubic $CsPbBr_3$ and $CsPbCl_3$ crystals are direct bandgap semiconductors.[25]

While some signals referring to Cs_4PbBr_6 (labeled with "*") still remain, as the $CrCl_3$ concentration increases, X-ray diffractogram is dominated by the $CsPbBr_xCl_{(3-x)}$ signals. Moreover, slight shift toward higher 2θ angles is expected since lattice parameter of the samples is reduced due to the $Br^- - Cl^-$ exchange and Cr^{+3} incorporation to the host lattice.[14]

To gain further insight into the influence of the dopant on the structure, further characterization on the structural properties is performed via SEM imaging. As presented in Figs. 1(b) and 1(e), in the case of undoped perovskite, two different structure types, which are distributed almost homogeneously, were spotted, ones having
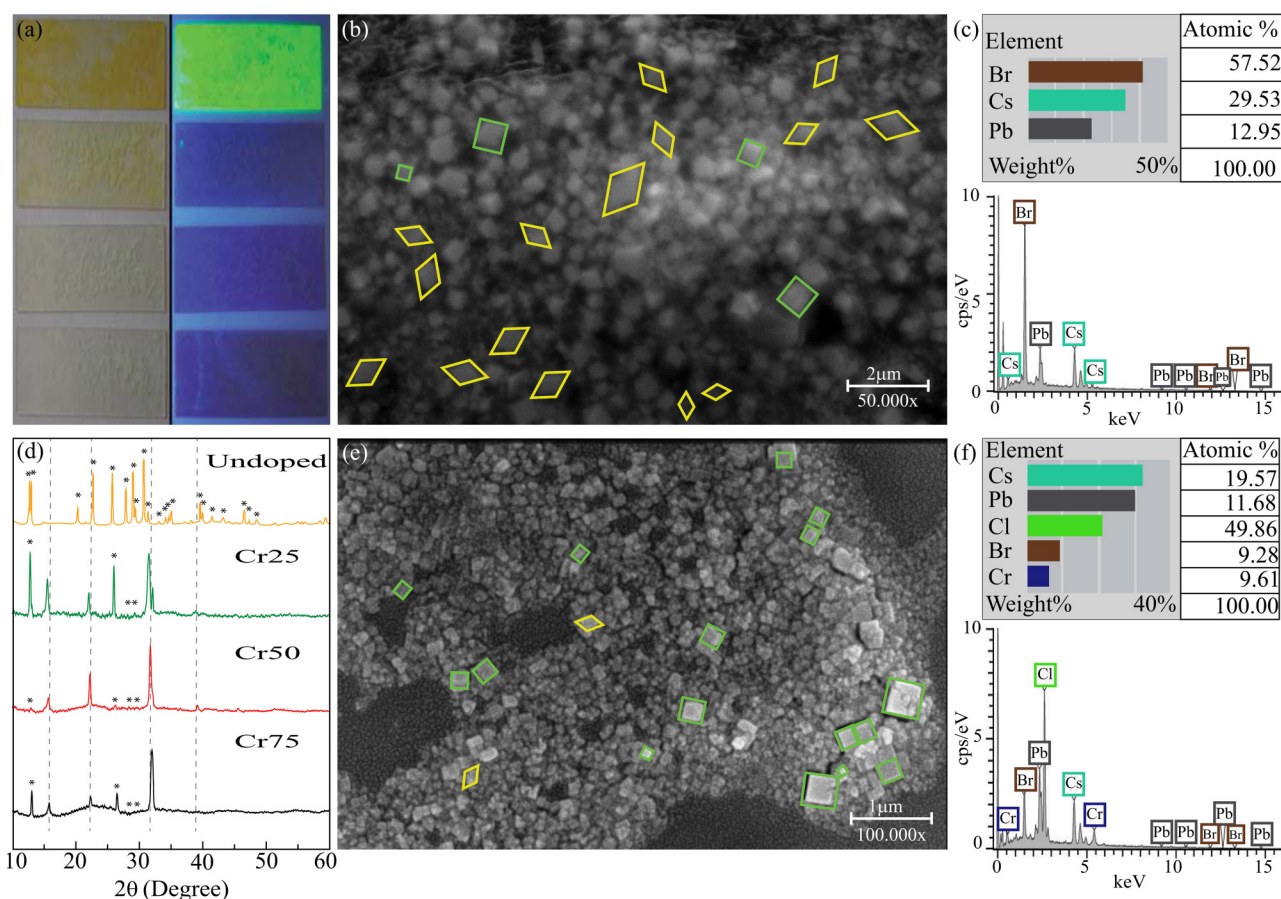

FIG. 1. (a) Photographic images (under daylight and UV), [(b) and (e)] SEM images of undoped and Cr75 samples, [(c) and (f)] energy dispersive X-ray (EDX) analysis of undoped and Cr75 samples, and (d) X-ray diffraction patterns of undoped, Cr25, Cr50, and Cr75 samples.

certain cubic symmetry highlighted by green regions and the others showing rhombus shape indicated with yellow rhombuses. As demonstrated by the XRD reflections, most of the sample is composed of Cs_4PbBr_6 crystals that have a rhombus-shaped primitive unit cell. In addition, lower panel of Figs. 1(b) and 1(e) shows that an increase in the Cr dopant leads to the formation of a significant amount of nanocrystals that are crystallized into the cubic phase indicating the presence of the $CsPbBr_xCl_{(3-x)}$ phase.

The corresponding EDX results of the undoped and Cr75 samples in the right column of Fig. 1 reveal that the undoped sample contains Br and Cs atoms, intensively hinting about the formation of Cs_4PbBr_6, where the amount of Br is the highest. On the other hand, Cr75 sample shows that there are also Cr atoms in addition to Cs, Pb, and Br atoms, which are found in relatively close amounts and higher than the amount of Cr. Since the more electronegative nature of Cl^- compared to Br^-, all Cr-doped perovskites contain various amounts of Cl^- in the host lattice. Therefore, stoichiometry of crystals as a result of anion exchange can be considered as follows: $CsPbBr_{1.41}Cl_{1.59}$:Cr for the Cr25 sample, $CsPbBr_{0.93}Cl_{2.07}$:Cr for the Cr50 sample, and $CsPbBr_{0.69}Cl_{2.31}$:Cr for the Cr75 sample. According to the EDX result of the Cr75 sample, the Cl:Br ratio is consistent with the calculated stoichiometric value.

The influence of the Cr dopants on the structural properties of $CsPbBr_3$ and $CsPbCl_3$ crystals, which are representative elements of the product of the synthesis, is also analyzed theoretically by performing state-of-the-art first-principles calculations. The structural analysis of undoped orthorhombic (Pnma) $CsPbBr_3$ and $CsPbCl_3$ crystals reveals that optimized lattice parameters are $a = 8.3$ Å, $b = 7.93$ Å, $c = 11.31$ Å and $a = 7.93$ Å, $b = 7.59$ Å, $c = 10.83$ Å, respectively. Each Pb atom in the $CsPbBr_3$ crystal bonds with six Br atoms with a bond length of 2.92 Å. Besides, in the $CsPbCl_3$ crystal, each Pb atom bonds with six Cl atoms with a bond length of 2.79 Å as seen in Fig. 2.

On the other hand, Cr-doping scenarios are also examined by means of total energy calculations. It is found that the Cr-Pb substitution is quite preferable for both $CsPbBr_3$ and $CsPbCl_3$. Thanks to substitutional doping of the chromium atom, $CsPbBr_3$ and $CsPbCl_3$ have 0.34 eV and 0.62 eV energy gain in doped structure. In addition, Cr-doping leads to 6.77% and 7.16% shrinkage in their lattice, respectively. Bader charge analysis shows that the Cr atom donates $1e$ and $1.2e$ to the host crystals $CsPbBr_3$ and $CsPbCl_3$, respectively, which is similar to the amount of charge donation of the Pb atom in the undoped case. However, the length of the bond between Pb and Br/Cl shortens, when the Cr atom is replaced with the Pb atom. Therefore, an increase in the charge density of the bond may strengthen the structure and provides extra stability.

In addition, theoretically predicted X-ray diffraction patterns of the bare $CsPbBr_3$ crystal and Cr-doped $CsPbBr_3$ are presented in Fig. 3. The characteristic reflection signals of the $CsPbBr_3$ appear at 15°, 22°, 31°, and 37° (2θ) marked with dashed lines. In the case of Cr-doping, no additional signal is observed due to the dopants; however, there is a certain shift toward higher 2θ values.

When the calculated and experimental reflection signals of bare perovskite NCs are compared, the characteristic ones of bare $CsPbBr_3$ overlap. Also, the shift of the signals of Cr-doped $CsPbBr_3$ NCs is observed in both calculated and experimentally obtained XRD patterns. The calculated and experimental results reveal that the Cr atoms that are placed in the host lattice by Pb-Cr substitutional doping cause a shrinkage in the lattice. Such shrinkage can also be seen in XRD peaks shifting to higher 2θ angles.

IV. ELECTRONIC AND OPTICAL PROPERTIES

Cr-doping procedure not only leads to the structural modification but also results in anomalous coloring emission of the perovskites. In this section, to understand the change in the emission,
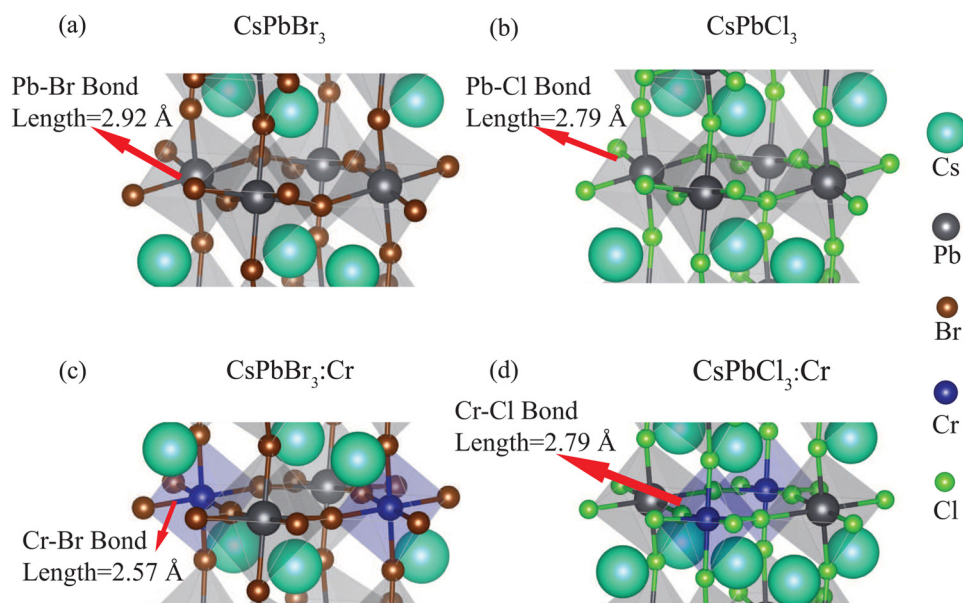

FIG. 2. Crystal structure of undoped (a) $CsPbBr_3$, (b) $CsPbCl_3$, Cr substituted for Pb in (c) $CsPbBr_3$ and (d) $CsPbCl_3$.
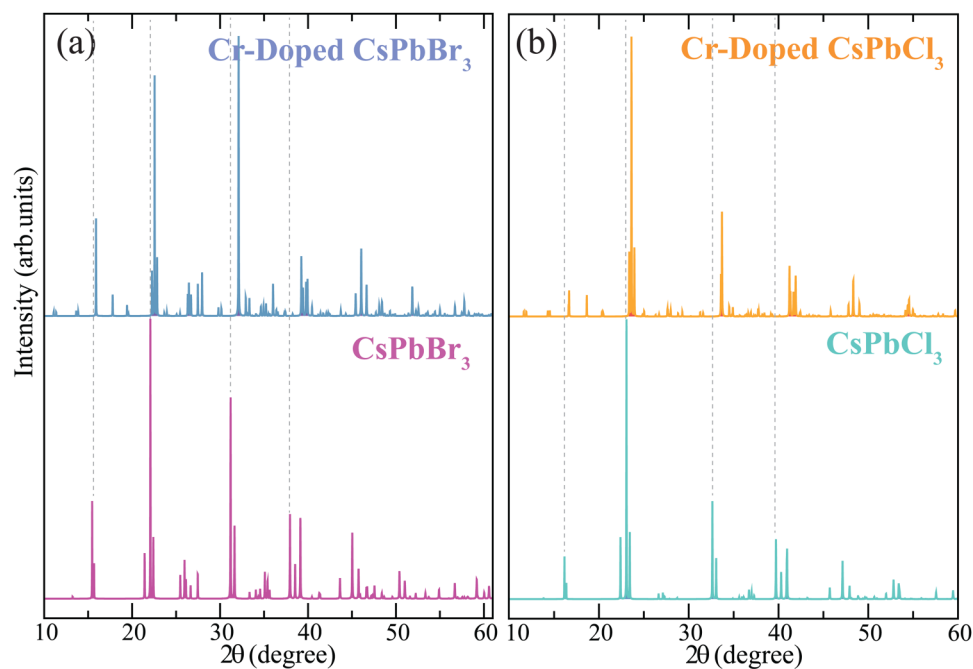
FIG. 3. Calculated XRD patterns of bare and doped (a) CsPbBr$_3$, (b) CsPbCl$_3$.

both optical measurements and electronic band dispersion calculations are performed.

The normalized UV-Vis photoluminescence (PL) spectrum of undoped and doped perovskite NCs is presented in Fig. 4(a). A single and sharp emission peak arises at 525 nm at the PL spectrum of the undoped sample, shown with a green solid line under the excitation of 254 nm UV light.

However, upon Cr-doping, the PL spectrum shown in Fig. 4(a) displays additional characteristic peaks between the 400 and

775 nm region. Since these peaks are localized at blue, green, and red areas of the visible spectrum and behave differently, the PL spectrum is divided into three sections and clarified separately.

The first group in the PL spectrum includes the peaks localized between 476 and 427 nm. As reported by Nedelcu et al., such a peak in the spectrum, which is strongly dependent on the CrCl$_3$ density, of cesium lead halide perovskites simply originates from the anion (Br$^-$−Cl$^-$) exchange.[13] Obviously, in our synthesis procedure, the increase in the amount of Cl$^-$ entering the system
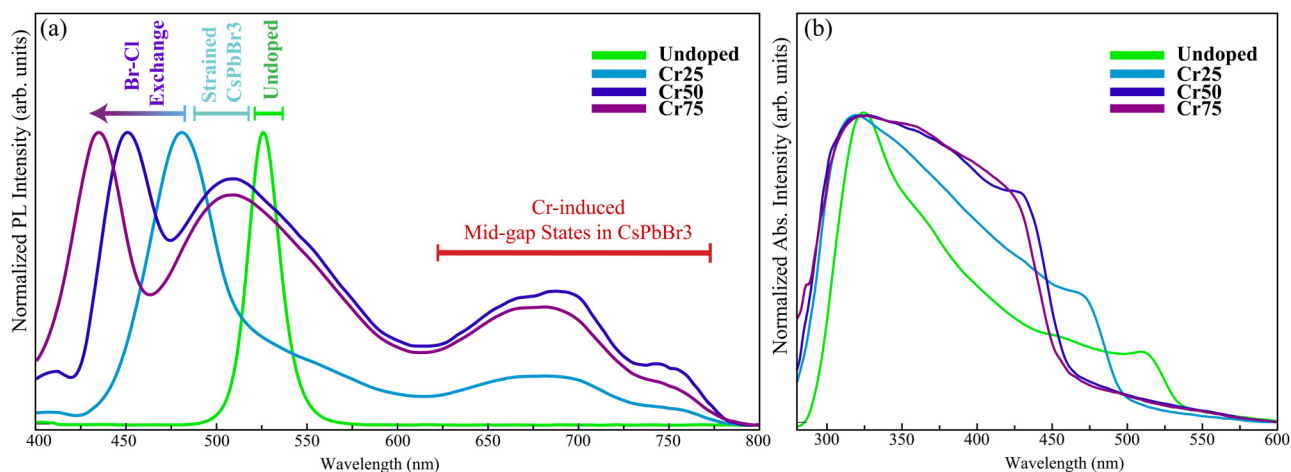

FIG. 4. Normalized (a) PL and (b) absorption spectrum of the undoped and doped samples with a concentration of 0.25 ml, 0.50 ml, and 0.75 ml.

during the doping process enables more anion exchange and, therefore, the larger the number of Cl ions in the host lattice, the higher the blue shift in the emission.

The second group in the PL spectrum is observed at the vicinity of 515 nm. While this peak emerges as a result of the doping, it is clearly independent from Cr concentration. As shown by DFT calculations, Pb-Cr substitution is energetically favorable and leads to slight shrinkage in the host lattice. As verified by our XRD measurements and DFT simulations, the existence of Cr dopants leads to shrinkage in the lattice of $CsPbBr_3$ and $CsPbCl_3$ (6.77% and 7.16%, respectively). Therefore, the bandgap that belongs to the host lattice increases and the emission peak shifts from 525 to 515 nm. Moreover, for dense doping cases in Cr50 and Cr75, its intensity increases to a certain extent as shown in Fig. 4(a). Here, it is worth noting that the presence of Cr dopants in the $CsPbBr_3$ host lattice acts as a barrier to the $Br^- - Cl^-$ exchange and is independent from the dopant solution concentration second peak appearing at the same wavelength.

In addition to these two regions in the PL spectrum, a third group that leads to broad emission peaks between 675 and 775 nm is also observed. Obviously, this region is formed upon Cr-doping and its intensity is increased with increasing dopant concentration. Electronic band dispersions shown in Fig. 5 reveal that both $CsPbBr_3$ and $CsPbCl_3$ perovskites display one broad and one narrow impurity bands in the whole Brillouin zone. This emission is originated from the Cr-induced midgap states, where electrons make radiative energy transitions.

Though the PL spectrum is quite a useful tool displaying the characteristics of semiconducting crystals allowing direct transitions, for identification and characterization of indirect bandgap semiconductors, the absorption spectrum provides a more reliable method. The normalized UV-Vis absorption spectra of the doped samples in the presence of varying $CrCl_3$ concentration is presented in Fig. 4(b) in comparison with the undoped sample. Regardless of doped or not, all samples show two sharp distinct excitonic absorption peaks. In the case of the undoped sample presented with a solid green line, the first absorption peak is located at 325 nm, which is sharper and has the highest absorption intensity, and the second one is located at the vicinity of 520 nm. The absorption spectrum of the undoped material reveals the formation of the Cs_4PbBr_6 phase[41,42] together with a trace amount of $CsPbBr_3$ phase, leading to a step at 520 nm.

Cr-doping also leads to significant modifications in the absorption spectrum. Upon increasing dopant solution concentration, a blue shift of the absorption edge from 510 toward 460 nm is also observed, while the position of the 325 nm peak changes negligibly (~10 nm). It is also seen that increasing the dopant ratio drives the second excitonic absorption peak toward the first one and a broad total absorption signal at 300–450 nm is formed. On the other hand, the absorption intensity of the second peak in doped samples shows a significant increase. As the intensity of the second peak increases due to the dopant concentration, the form of the absorption spectrum recorded from our samples begins to resemble the $CsPbBr_3$ NC spectrum.[43] We attribute this increase to a rise in the amount of
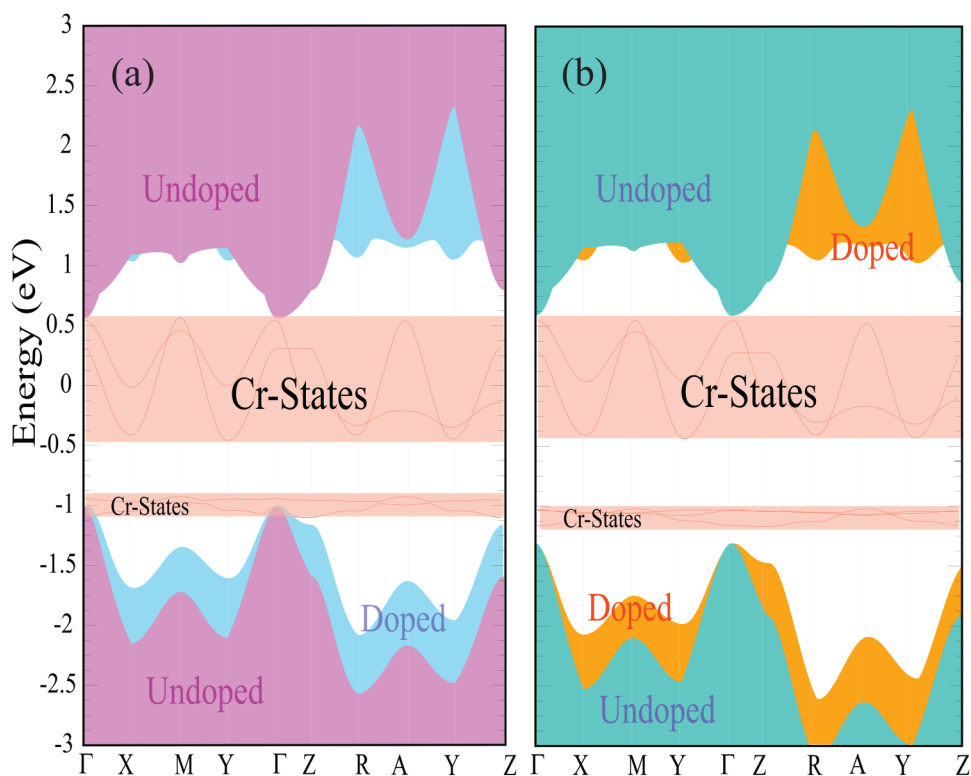

FIG. 5. Electronic band dispersion of Cr-doped and undoped (a) $CsPbBr_3$ and (b) $CsPbCl_3$. Fermi levels are set to zero.
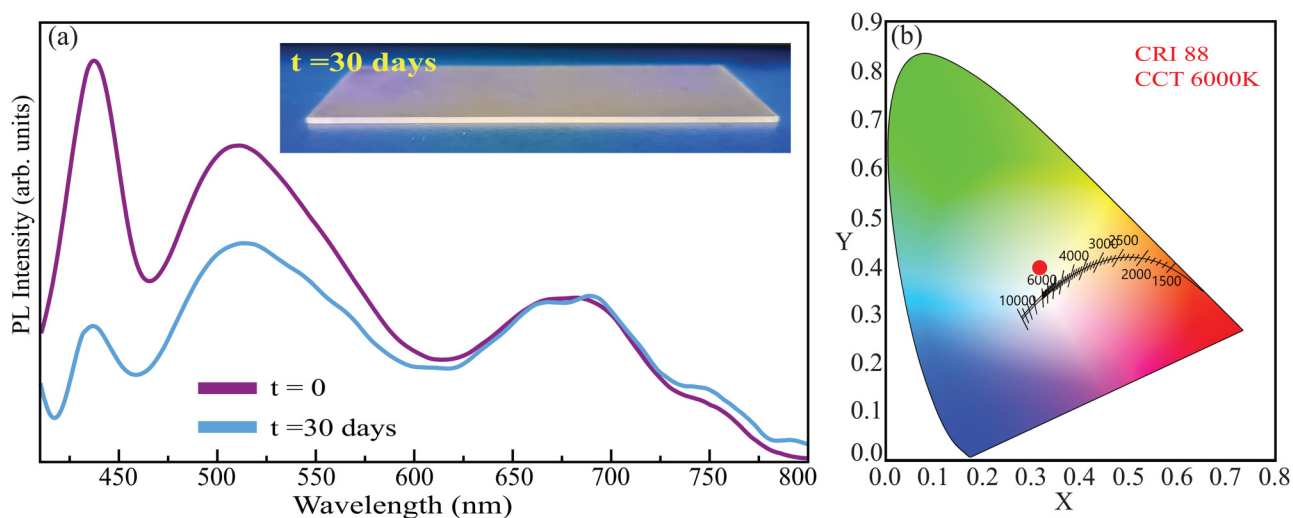
FIG. 6. Photoluminescence spectrum of the Cr75 sample (a) at $t = 0$ and $t = 30$ days. Inset: the photographic image of the sample under 254 nm UV light and (b) plotted on the CIE diagram at $t = 30$ days.

the nanocrystals that are crystallized in a cubic shape, which refers to the $CsPbBr_3$ phase.

V. COLOR CHANGE AND SINGLE-PHASE WHITE LIGHT GENERATION

Although there is no visible change in the macroscopic structure, interaction with environment leads to significant modifications in the electronic and optical properties. While the structure initially emits violaceous color due to the excessive amount of Cl ions, the emission color of Cr-doped lead halide perovskites explicitly turns into white after 30 days. This intensity change in time was tracked by collecting their PL in time and presented in Fig. 6. The PL spectrum of the doped perovskite reveals that the intensity of the peaks originates from the halide exchange region (bluish emission) and from compressively strained Cr-free (greenish emission) decrease in time and eventually becomes comparable to the intensity of peaks originating from the Cr-induced impurity states. Therefore, it is expected to observe white color since the intensity of these three PL groups becomes comparable.

In addition, our DFT simulations show that water molecules can penetrate into the host lattice of doped and undoped perovskites of $CsPbCl_3$ and $CsPbBr_3$ without seeing any energy barrier. Adsorption energy per H_2O molecule is calculated to be 190, 420, and 150 meV for $CsPbBr_3$, $CsPbCl_3$, and Cr-doped $CsPbBr_3$, respectively. Apparently, the Br-Cl exchanged perovskite domains strongly interact with H_2O molecules, and, therefore, emission that originates from the $CsPbBr_xCl_{3-x}$ crystals dramatically decreases in time due to moisture.

Commission Internationale de l'Eclairage (CIE) chromaticity diagram shown in Fig. 6(b) precisely characterizes colors by a luminance parameter and two color coordinates x and y. Chromaticity curve surrounding all the colors perceivable by a normal human

eye shows that the red circle located at the color coordinates of (0.3161, 0.3938) confirms the generation of white light which is close to the coordinates for pure white light (0.3333, 0.3333). Furthermore, this sample shows high Color Rendering Index (CRI) of 88 and Correlated Color Temperature (CCT) of 6000 K indicating that it is commercially viable.

VI. CONCLUSIONS

In summary, Cr-doped mixed halide perovskites have been obtained by following a facile route involving the antisolvent recrystallization method at room temperature. Structural characterization confirms that there is a phase transition from Cs_4PbBr_6 to $CsPbBr_xCl_{3-x}$ when the dopant is introduced, and DFT calculations verify this phase transition by indicating that it is favorable. On the other hand, incorporation of the Cr^{3+} ions into the lattice forms multiple emission peaks, which are identified as they appear due to strained lattice, and forms midgap states. Interestingly, due to the strong interaction of the mixed halide perovskite domains with the moisture, the PL intensity corresponding to $CsPbBr_xCl_{3-x}$ crystals is reduced dramatically in time, and Cr-doped halide perovskite samples then start to exhibit clear white light emission with a high CRI. Our results reveal that Cr-doped all-inorganic perovskites are promising candidates for single-phase white light sources with high quantum efficiency.

SUPPLEMENTARY MATERIAL

See the supplementary material including computational details for indentation of the water molecule through the doped and undoped $CsPbX_3$ (X = Cl, Br) surfaces.

REFERENCES

[1] Q. Dong, Y. Fang, Y. Shao, P. Mulligan, J. Qiu, L. Cao, and J. Huang, Science **347**, 967–970 (2015).

[2] K. Wu, G. Liang, Q. Shang, Y. Ren, D. Kong, and T. Lian, J. Am. Chem. Soc. **137**, 12792–12795 (2015).

[3] S.-T. Ha, R. Su, J. Xing, Q. Zhang, and Q. Xiong, Chem. Sci. **8**, 2522–2536 (2017).

[4] L. Protesescu, S. Yakunin, M. I. Bodnarchuk, F. Krieg, R. Caputo, C. H. Hendon, R. X. Yang, A. Walsh, and M. V. Kovalenko, Nano Lett. **15**, 3692–3696 (2015).

[5] J. Song, J. Li, X. Li, L. Xu, Y. Dong, and H. Zeng, Adv. Mater. **27**, 7162–7167 (2015).

[6] T. Guner and M. M. Demir, Phys. Status Solidi A **215**, 1800120 (2018).

[7] X. He, Y. Qiu, and S. Yang, Adv. Mater. **29**, 1700775 (2017).

[8] H. Huang, L. Polavarapu, J. A. Sichert, A. S. Susha, A. S. Urban, and A. L. Rogach, NPG Asia Mater. **8**, e328 (2016).

[9] M. V. Kovalenko, L. Protesescu, and M. I. Bodnarchuk, Science **358**, 745–750 (2017).

[10] C. C. Stoumpos, C. D. Malliakas, J. A. Peters, Z. Liu, M. Sebastian, J. Im, T. C. Chasapis, A. C. Wibowo, D. Y. Chung, A. J. Freeman et al., Cryst. Growth Des. **13**, 2722–2727 (2013).

[11] X. Li, F. Cao, D. Yu, J. Chen, Z. Sun, Y. Shen, Y. Zhu, L. Wang, Y. Wei, Y. Wu et al., Small **13**, 1603996 (2017).

[12] K.-H. Wang, L. Wu, L. Li, H.-B. Yao, H.-S. Qian, and S.-H. Yu, Angew. Chem. Int. Ed. **55**, 8328–8332 (2016).

[13] G. Nedelcu, L. Protesescu, S. Yakunin, M. I. Bodnarchuk, M. J. Grotevent, and M. V. Kovalenko, Nano Lett. **15**, 5635–5640 (2015).

[14] Q. A. Akkerman, V. D'Innocenzo, S. Accornero, A. Scarpellini, A. Petrozza, M. Prato, and L. Manna, J. Am. Chem. Soc. **137**, 10276–10281 (2015).

[15] S. Pathak, N. Sakai, F. Wisnivesky Rocca Rivarola, S. D. Stranks, J. Liu, G. E. Eperon, C. Ducati, K. Wojciechowski, J. T. Griffiths, A. A. Haghighirad et al., Chem. Mater. **27**, 8066–8075 (2015).

[16] N. Pellet, P. Gao, G. Gregori, T.-Y. Yang, M. K. Nazeeruddin, J. Maier, and M. Grätzel, Angew. Chem. **126**, 3215–3221 (2014).

[17] D. Bi, W. Tress, M. I. Dar, P. Gao, J. Luo, C. Renevier, K. Schenk, A. Abate, F. Giordano, J.-P. C. Baena et al., Sci. Adv. **2**, e1501170 (2016).

[18] G. Pan, X. Bai, D. Yang, X. Chen, P. Jing, S. Qu, L. Zhang, D. Zhou, J. Zhu, W. Xu et al., Nano Lett. **17**, 8005–8011 (2017).

[19] A. K. Guria, S. K. Dutta, S. D. Adhikari, and N. Pradhan, ACS Energy Lett. **2**, 1014–1021 (2017).

[20] Q. Hu, Z. Li, Z. Tan, H. Song, C. Ge, G. Niu, J. Han, and J. Tang, Adv. Opt. Mater. **6**, 1700864 (2018).

[21] M. Liu, G. Zhong, Y. Yin, J. Miao, K. Li, C. Wang, X. Xu, C. Shen, and H. Meng, Adv. Sci. **4**, 1700335 (2017).

[22] Y. Zhou, J. Chen, O. M. Bakr, and H.-T. Sun, Chem. Mater. **30**, 6589 (2018).

[23] W. Liu, Q. Lin, H. Li, K. Wu, I. Robel, J. M. Pietryga, and V. I. Klimov, J. Am. Chem. Soc. **138**, 14954–14961 (2016).

[24] A. Swarnkar, V. K. Ravi, and A. Nag, ACS Energy Lett. **2**, 1089–1098 (2017).

[25] T. Guner, B. Akbali, M. Ozcan, G. Topcu, M. M. Demir, and H. Sahin, J. Phys. Chem. C **122**, 11543 (2018).

[26] J. Navas, A. Sánchez-Coronilla, J. J. Gallardo, N. C. Hernández, J. C. Piñero, R. Alcántara, C. Fernández-Lorenzo, M. Desireé, T. Aguilar, and J. Martín-Calleja, Nanoscale **7**, 6216 (2015).

[27] A. L. Abdelhady, M. I. Saidaminov, B. Murali, V. Adinolfi, O. Voznyy, K. Katsiev, E. Alarousu, R. Comin, I. Dursun, L. Sinatra et al., J. Phys. Chem. Lett. **7**, 295 (2016).

[28] K.-T. Kim and C.-Il Kim, Thin Solid Films **472**, 26 (2005).

[29] A. Banerjee, S Pal, and B. K. Chaudhuri, J. Chem. Phys. **115**, 1550 (2001).

[30] S. Shen, J. Jiang, P. Guo, C. X. Kronawitter, S. S. Mao, and L. Guo, Nano Energy **1**, 732 (2012).

[31] R. Bhatt, S. Kar, K. S. Bartwal, and V. K. Wadhawan, Solid State Commun. **127**, 457 (2003).

[32] X. Li, Y. Wu, S. Zhang, B. Cai, Y. Gu, J. Song, and H. Zeng, Adv. Funct. Mater. **26**, 2435–2445 (2016).

[33] J. Zhu, X. Yang, Y. Zhu, Y. Wang, J. Cai, J. Shen, L. Sun, and C. Li, J. Phys. Chem. Lett. **8**, 4167–4171 (2017).

[34] G. Kresse and J. Furthmüller, Phys. Rev. B **54**, 11169 (1996).

[35] G. Kresse and J. Hafner, Phys. Rev. B **47**, 558 (1993).

[36] G. Kresse and D. Joubert, Phys. Rev. B **59**, 1758 (1999).

[37] P. E. Blöchl, Phys. Rev. B **50**, 17953 (1994).

[38] J. P. Perdew and A. Zunger, Phys. Rev. B **23**, 5048 (1981).

[39] D. M. Ceperley and B. Alder, Phys. Rev. Lett. **45**, 566 (1980).

[40] G. Henkelman, A. Arnaldsson, and H. Jónsson, Comput. Mater. Sci. **36**, 354 (2006).

[41] M. I. Saidaminov, J. Almutlaq, S. Sarmah, I. Dursun, A. A. Zhumekenov, R. Begum, J. Pan, N. Cho, O. F. Mohammed, and O. M. Bakr, ACS Energy Lett. **1**, 840–845 (2016).

[42] Y. Zhang, M. I. Saidaminov, I. Dursun, H. Yang, B. Murali, E. Alarousu, E. Yengel, B. A. Alshankiti, O. M. Bakr, and O. F. Mohammed, J. Phys. Chem. Lett. **8**, 961–965 (2017).

[43] Z. Hu, Z. Liu, Y. Bian, D. Liu, X. Tang, W. Hu, Z. Zang, M. Zhou, L. Sun, J. Tang et al., Adv. Opt. Mater. **5**, 1700419 (2017).